Fractography Analysis of 1.0 wt% Nanoclay/ Multi-Layer Graphene Reinforced Epoxy Nanocomposites

Rasheed Atif and Fawad Inam*

Northumbria University, Faculty of Engineering and Environment, Department of Mechanical and Construction Engineering, Newcastle upon Tyne NE1 8ST, United Kingdom.

E-mail: fawad.inam@northumbria.ac.uk (Tel.: +44 1912273741)

Abstract: The topographical features of fractured tensile, flexural, K_{1C}, and impact specimens of 1.0 wt% Multi-Layer Graphene (MLG)/nanoclay-epoxy (EP) nanocomposites have been investigated. The topographical features studied include maximum roughness height (R_{max} or R_z), root mean square value (R_q), roughness average (R_a), and waviness (W_a). Due to deflection and bifurcation of the cracks by nanofillers, specific fracture patterns are observed. Although these fracture patterns seem aesthetically appealing, however, if delved deeper, they can further be used to estimate the influence of nanofiller on the mechanical properties. By a meticulous examination of topographical features of fractured patterns, various important aspects related to fillers can be approximated such as dispersion state, interfacial interactions, presence of agglomerates, and overall influence of the incorporation of filler on the mechanical properties of nanocomposites. In addition, treating the nanocomposites with surfaces of specific topography can help improve the mechanical properties of nanocomposites.

Key words: Fractography; Multi-Layer Graphene (MLG); Nanoclay; Epoxy; Nanocomposites.

1 Introduction:

The polymer matrix composites (PMCs) are commonly used in construction, automotive, and aerospace mainly because of high strength to weight ratio [1–3]. In PMCs, thermosetting epoxy is the most commonly used matrix [4–7]. The damage tolerance and fracture toughness of epoxy can be enhanced with the incorporation of (nano-) fillers such as metallic oxides [8–10], clays [11–13], carbon nanotubes (CNTs) [14–16], and other carbonaceous materials [17–19,6,5]. When nanofillers are introduced in polymers, the fracture pattern significantly changes due to the defection of advancing cracks with strong nanofillers. The topography of fractured surfaces can provide information about the dispersion state of nanofillers and interfacial interactions. There are two main classifications of topography measurement methods: non-contact techniques, such as focus-follow method, and contact techniques, such as stylus method [20]. Non-contact techniques have found more applications than contact techniques. In case of fragile surfaces, non-contact techniques are especially preferred as damage to surface may occur if contacted. In both the classifications, the parameter definitions remain the same. The results obtained by two techniques are also alike. The non-contact techniques do not only keep the surface under examination intact, but also the topography can be measured easily and quickly. However, these techniques have certain limitations. For example, those regions of surface which are not in the line of sight may not be detected by some non-contact techniques resulting in artefacts. In addition, due to the non-uniform intensity of light, the focus lens may follow the surface inaccurately resulting in the erroneous results. Furthermore, as there is no external agency to interact with the surface, the topography results will be exactly the replica of the surface under examination. At one side, it is an advantage. On the other hand, it may produce artefacts in the results. For example, if the surface contains contaminations, such as dirt, the contaminations will appear in topography profile. This effect may be well pronounced at nano-scale. Therefore, the samples should be prepared meticulously for non-contact techniques.

In current work, Multi-Layered Graphene (MLG)/nanoclay-epoxy nanocomposites of three different types were produced: (1) 1.0 wt% MLG-EP, (2) 1.0 wt% clay-EP, and (3) 0.5 wt% MLG-0.5 wt% clay-EP. The maximum enhancement in mechanical properties was recorded in 0.5 wt% MLG-0.5 wt% clay-EP nanocomposites, especially when treated with 1200P abrasive paper. The second highest improvement in mechanical properties was observed in case of 1.0 wt% MLG-EP nanocomposites. However, in case of 1.0 wt% clay-EP, least improvement in mechanical properties was observed. It can be attributed to the interfacial interactions and presence of agglomerates that cause

stress concentration and concomitant degradation of mechanical properties [3]. The fractography analysis of the samples revealed that nanofillers significantly influence the fracture patterns. In addition, a careful examination of the topographical features of the fractured surfaces suggests that the dispersion state of the fillers, interfacial interactions, and presence of any agglomerates of filler can be estimated based on the surface parameters such as maximum surface roughness (R_z or R_{max}), surface roughness average (R_a), and root mean square parameter of roughness (R_q). For example, a high value of R_z (with low R_a value) with deep crater and/or trenches indicates the presence of filler agglomerates and concomitant poor mechanical properties of polymer nanocomposites. Similarly, a relatively high surface roughness average with low R_z value indicates the uniform dispersion of the filler and simultaneously improved mechanical properties. However, it was observed that waviness average parameter (W_a) does not have any relation with the weight fraction, dispersion state, or agglomeration of the filler.

2 Experimental work:

2.1 Materials:

MLG (99.2% purity, 80 m^2/g specific surface area, 4.5 μm average lateral size, 12 nm average thickness) used was purchased from Graphene Supermarket, USA. Halloysite nanoclay was used as second filler and purchased from Sigma-Aldrich. The diameter of the nanoclay is between 30-70 nm with length 1-4 μm and has a tube-like morphology. The density of the nanoclay is 2.53 g/cm^3 and surface area is 64 m^2/g. The epoxy and hardeners used were based on bisphenol A-epichlorohydrin and dimethylbenzylamine isophorone diamine, respectively. The resin was purchased from Polyfibre, UK. The densities of liquid epoxy and hardener were ~1.3 g/cm^3 and ~1.1 g/cm^3, respectively.

2.2 Production of samples:

The nanofillers were dispersed in the hardener using tip sonicator (Model VC 750, Vibra-cell, USA, 750 W, 250 kHz). Although the sonication was carried out at room temperature, however, temperature of the system rose due to high energy vibrations produced by tip sonicator. The resins were vacuum degassed in separate beakers for 30 min. Then, the resins were mixed manually for 10 min. The mixing ratio (by weight) of hardener: epoxy was 1:2. The mixture was again degassed for 15 min. The samples were cast in silicone molds. Two-step curing was carried out: room temperature for 6 h and post-curing at 150 °C for overnight.

2.3 Characterization:

An Infinite focus Alicona G4 optical microscope was employed to measure topography. The working principle of the microscope is focus-follow method which is a non-contact method. Universal Testing Machine (Instron Model 3382) was used to conduct tensile test (ASTM D638, 4 mm thickness, Type-V geometry, 0.5 mm/min), three-point bending test (ASTM D790, 3 × 12.7 × 48 mm, 1.0 mm/min), and mode-I fracture toughness test (ASTM D5045, 36 × 6 × 3 mm, crack length 3 mm, 0.5 mm/min). ASTM standard D 6110 was used to measure Charpy impact toughness (specimen dimensions 64 × 12.7 × 3.2 mm with V-notch of 45°, 2.5 mm depth and 0.25 mm tip of radius). The schematics of specimens are presented in Figure 1.

3 Results and discussion:

The mechanical properties have been summarized in Table 1. The densification of samples was around 99.5% and weight loss by treating abrasive papers was highest in case of 60P abrasive paper (16%). The microhardness increased in case of nanocomposites processed with velvet cloth and 1200P paper and decreased when samples were processed with 320P and 60P abrasive papers. The maximum microhardness was recorded in case of 0.5 wt% MLG-0.5 wt% nanoclay-EP nanocomposites. The Young's modulus increased in all cases when samples were processed with 1200P abrasive paper and velvet cloth. However, the stiffness decreased when the nanocomposites were processed with 320P and 60P abrasive papers. The values indicate that stiffness can be enhanced by processing the nanocomposites with velvet cloth and 1200P paper and decreased by processing the nanocomposites with 320P and 60P papers. The maximum increase in Young's modulus was observed in case of 0.5 wt% MLG-0.5 wt% nanoclay-EP nanocomposites and in case of nanocomposites processed with 1200P abrasive paper. The UTS also increased in all cases when nanocomposites were processed with 1200P abrasive paper and velvet cloth. However, UTS decreased when the nanocomposites were processed with 60P and 320P abrasive papers. The values show that UTS can be improved by treating the nanocomposites with 1200P abrasive paper and velvet cloth and decreased by treating the nanocomposites

with 60P and 320P abrasive papers. The maximum increase in UTS was observed in case of 0.5 wt% MLG-0.5 wt% nanoclay-EP nanocomposites processed with 1200P abrasive paper. The tensile strain increased with high surface roughness values. It can be because of the reduction in strength and stiffness values. The treatment with velvet cloth did not show any visible change in tensile strain. However, the tensile strain slightly increased when the nanocomposites were processed with 1200P abrasive paper. Similar results were shown by nanocomposites when tested for flexural properties. The values indicate that from the three compositions made with five surface conditions for each composition, the best combination of mechanical performance can be achieved in case of 0.5 wt% MLG-0.5 wt% nanoclay-EP nanocomposites processed with 1200P abrasive paper. The K_{1C} remained impervious to any variation in topography. However, the standard deviation is not the same. It can be explained on the basis of tip of notch. A razor blade was used to sharpen the tip of notch that may not create tips of equal curvature and length. The other factor can be distribution, size, and volume fraction of porosity influencing the mechanical performance of nanocomposites. The G_{1C} increased with increasing surface roughness values. However, as K_{1C} remained impervious to topography, therefore, the variation in G_{1C} should not be a result of the variation in the topography. K_{1C}^2 was divided by stiffness to calculate G_{1C}. As stiffness decreased with increasing surface roughness values, therefore, a high value of G_{1C} resulted by increasing surface roughness. Although K_{1C} remained impervious to any variation in topography, however, topography showed a pronounced impact on impact toughness indicating that topography is more influential under impact loading.

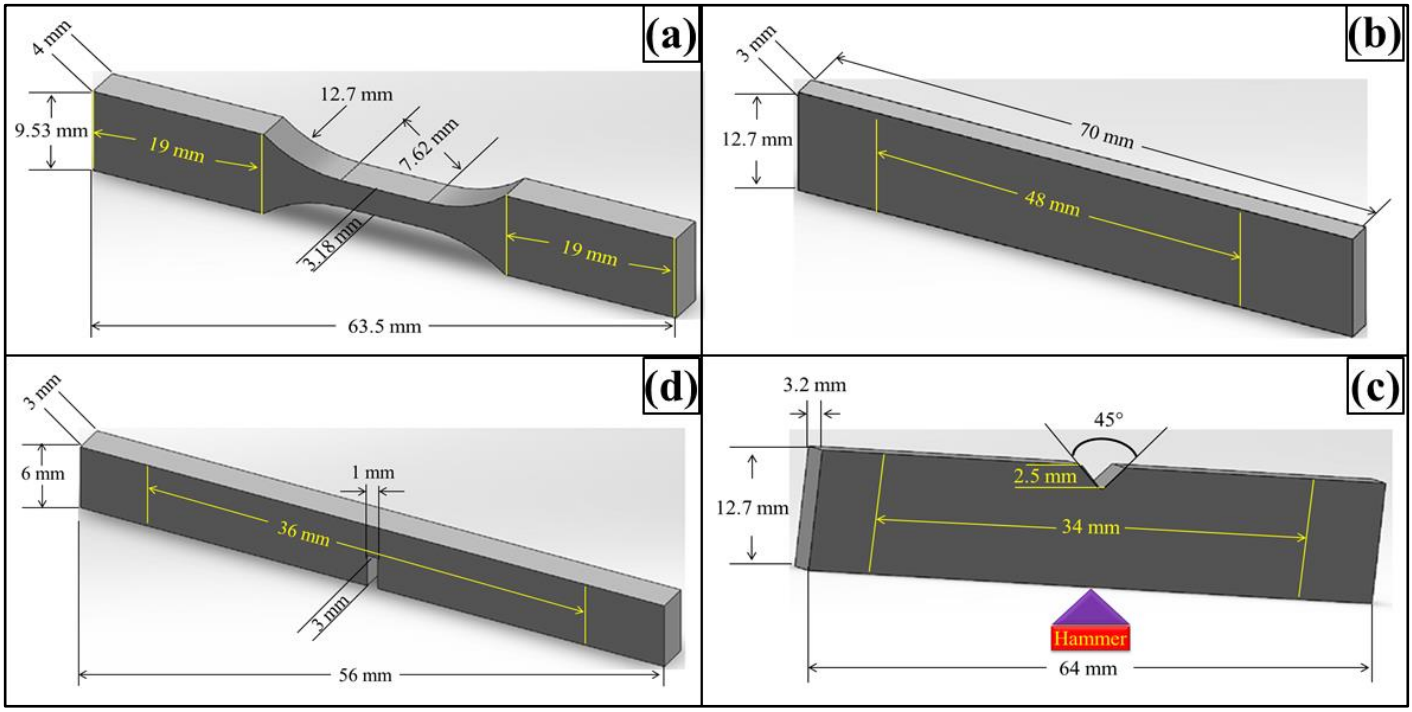

Figure 1: Schematics of mechanical test specimens: (a) tensile, (b) three-point bending, (c) Charpy impact toughness, and (d) fracture toughness.

The fractography surfaces of 1.0 wt% MLG-EP nanocomposites are shown in Figure 2. The monolithic epoxy shows straight bamboo-like fracture pattern indicating the occurrence of typical epoxy brittle fracture. However, with the incorporation of carbonaceous reinforcements, the cracks are rebounded resulting in non-linear and parabolic fracture patterns [21]. This was the reason that no specific orientation of crack propagation was observed in 3PBT specimens reinforced with MLG. The fracture became coarser when the samples were treated with 1200P abrasive paper and velvet cloth while trenches and straight and flat fracture patterns were observed when the samples were treated with 60P and 320P abrasive papers. The fracture patterns of K_{1C} specimens differ from those of 3PBT specimens in a way that fracture was originated from the notch tip as the tip generated high levels of stress concentration. As the displacement rate is relatively low in K_{1C} testing, the surface notches showed a significant impact on the topography of fracture surfaces. However, the influence of surface notches and topographical features on fracture patterns was marginalized in case of Charpy impact testing where the samples were suddenly impacted at the back of the notch by a

heavy and pointed hammer. Sheer and straight fracture patterns were observed in Charpy impact specimens and fracture took place right from the tip of notch.

Table 1: Mechanical properties of 1.0 wt% MLG/nanoclay-EP nanocomposites.

Sr.	Properties	As-cast	Velvet cloth	1200P	320P	60P
1	Densification (%)	99.3 ± 0.34	99.3 ± 0.31	99.4 ± 0.30	99.4 ± 0.32	99.3 ± 0.36
		99.4 ± 0.35	99.4 ± 0.32	99.5 ± 0.33	99.2 ± 0.31	99.4 ± 0.33
		99.4 ± 0.38	99.4 ± 0.31	99.4 ± 0.31	99.3 ± 0.41	99.3 ± 0.34
2	Microhardness (HV)	368 ± 15.2	385.1 ± 10.2	403.4 ± 11.8	344 ± 18.6	301 ± 21.7
		342.3 ± 21.6	374.9 ± 18.3	395.8 ± 9.0	331.5 ± 18.1	326.2 ± 31.4
		379.9 ± 21.2	382.1 ± 19.2	413.3 ± 18.8	354.9 ± 18.6	316.9 ± 21.7
3	Young's modulus (MPa)	834.5 ± 29.5	842.8 ± 24.5	875.1 ± 28.5	804 ± 35.9	794.2 ± 42.6
		757.4 ± 22.1	790.4 ± 17.6	809.7 ± 23.6	751.2 ± 28.9	720.4 ± 33.8
		862.5 ± 18.9	873.8 ± 16.8	898 ± 19.5	826 ± 23.4	818.9 ± 28.6
4	UTS (MPa)	74.4 ± 1.5	76.7 ± 2.1	82.2 ± 1.6	69.7 ± 1.8	65.3 ± 2.5
		62.4 ± 1.1	66.5 ± 1.2	72.4 ± 1.3	62.7 ± 2.1	60.6 ± 3.6
		78.2 ± 1.2	80.4 ± 1.7	86.1 ± 1.9	73.4 ± 2.9	69.6 ± 3.1
5	Tensile strain (%)	6.8 ± 1.1	6.2 ± 0.9	6.7 ± 1.6	7.4 ± 1.2	8.1 ± 2.1
		9.2 ± 0.9	9.6 ± 0.8	10.2 ± 0.8	10.1 ± 1.1	13.4 ± 1.8
		6.8 ± 0.8	5.2 ± 0.9	6.2 ± 0.7	7.4 ± 1.3	7.6 ± 1.8
6	Flex. Modulus (MPa)	808.3 ± 38.3	896.1 ± 25.3	904.3 ± 30.5	877.9 ± 33.5	669.9 ± 42.6
		745.4 ± 32.7	847.8 ± 22.5	875.1 ± 33.4	824.4 ± 34.4	633.7 ± 43.4
		842.6 ± 31.4	934.1 ± 26.2	946.3 ± 31.4	901.8 ± 37.5	696.9 ± 32.6
7	Flex. Strength (MPa)	88.7 ± 6.9	91.4 ± 3.8	99 ± 2.9	85.3 ± 4.6	83.4 ± 8.3
		76.1 ± 5.3	83.5 ± 4.5	95.6 ± 4.4	81.4 ± 6.6	72.2 ± 8.7
		91.5 ± 3.5	94.7 ± 3.1	98.3 ± 2.6	90.3 ± 8.5	89.5 ± 10.7
8	Flex. Strain (%)	4.7 ± 0.06	4.6 ± 0.29	4.4 ± 0.31	5.1 ± 0.49	5.4 ± 0.4
		5.2 ± 0.08	5.4 ± 0.12	5.9 ± 0.13	5.2 ± 0.21	6.4 ± 0.29
		4.2 ± 0.05	4.7 ± 0.08	4.5 ± 0.09	4.4 ± 0.12	5.3 ± 0.19
9	K_{1C} (MPa·m$^{1/2}$)	1.27 ± 0.1	1.23 ± 0.15	1.25 ± 0.05	1.21 ± 0.1	1.2 ± 0.1
		0.97 ± 0.08	0.84 ± 0.09	1.01 ± 0.11	0.93 ± 0.13	0.91 ± 0.17
		1.22 ± 0.07	1.26 ± 0.08	1.24 ± 0.09	1.25 ± 0.11	1.21 ± 0.13
10	G_{1C} (J/m^2)	352.5 ± 51.5	554.6 ± 42.3	656.5 ± 47.9	657.7 ± 62.8	769.1 ± 69.8
		322.2 ± 31.6	532.3 ± 26.3	598.2 ± 22.3	642.1 ± 41.5	756.3 ± 48.6
		374.4 ± 29.3	587.6 ± 28.6	653.5 ± 22.6	715.6 ± 38.9	794.6 ± 43.4
11	Charpy (kJ/m^2)	1.42 ± 0.15	1.54 ± 0.1	1.63 ± 0.09	1.31 ± 0.12	1.28 ± 0.2
		1.33 ± 0.11	1.54 ± 0.09	1.44 ± 0.09	1.27 ± 0.11	1.29 ± 0.17
		1.43 ± 0.09	1.54 ± 0.08	1.72 ± 0.1	1.34 ± 0.13	1.31 ± 0.19

The fractography surfaces of 1.0 wt% clay-EP nanocomposites are shown in Figure 3. Overall, a coarser topography of fractured surfaces was observed in 1.0 wt% MLG-EP samples than in 1.0 wt% clay-EP samples. No specific orientation of crack propagation was recorded in 3PBT specimens reinforced with nanoclay. As in case of 1.0 wt% MLG-EP samples, the fracture patterns of K_{1C} specimens of 1.0 wt% clay-EP samples differ from those of 3PBT specimens in a way that fracture was originated from the notch tip as the tip generated high levels of stress

concentration. As the displacement rate is relatively low in K_{1C} testing, nanoclay also showed a significant impact on the topography of fracture surfaces. However, the influence of nanoclay on fracture patterns was marginalized in case of Charpy impact testing where the samples were suddenly impacted at the back of the notch by a heavy and pointed hammer. Sheer and straight fracture patterns were observed in Charpy impact specimens and fracture took place right from the tip of notch. The fractography surfaces of 0.5 wt% MLG-0.5 wt% clay-EP nanocomposites are shown in Figure 4. Overall, the coarsest topography of fractured surfaces was observed in case of 0.5 wt% MLG-0.5 wt% clay-EP nanocomposites. The details of topographical features are further discussed below.

The topographical features of fracture surfaces of tensile specimen of 1.0 wt% MLG/clay-EP nanocomposites are shown in Figure 5-7. The surface waviness (Figure 5-7ii) and Gaussian distribution (Figure 5-7iv) did not show a specific trend of change with the abrasive papers. It can be attributed to the multiple factors affecting the fracture pattern such as surface notches, MLG/clay distribution, orientation, and interfacial interactions. Usually a specific pattern is observed in waviness due to wobbling of machining tool. On the contrary to W_a, a specific variation in surface roughness (Figure 5-7iii) was observed. The surface roughness of as-cast 1.0 wt% MLG-EP nanocomposites varied between ±6 µm with the presence of deep crests and troughs. With the treatment with the velvet cloth, the surface roughness changed slightly which became pronounced in samples treated with 1200P abrasive paper. However, in case of samples treated with 60P and 320P abrasive papers, deep trenches can be observed in roughness patterns (Figure 5-7diii and Figure 5-7eiii) that may be attributed to the presence of large notches. The trenches can also be observed in the surface profiles (Figure 5-7dv and Figure 5-7ev).

The topographical features are summarized in Figure 8. This R_z comes from the ravines formed due to brittle fracture in the thermoset. The R_z values were significantly decreased by the incorporation of nanofillers. As ravines present in monolithic epoxy are removed with the incorporation of nanofillers due to the diversion of advancing cracks, therefore, a decrease in R_z indicates a uniform dispersion of fillers and deflection of the cracks. In addition, an increase in mechanical properties with the incorporation of nanofillers further corroborates the uniform dispersion of nanofillers and energy dissipation at deflection of cracks. The variation in R_z value is in accord with the change in the mechanical properties. Therefore, R_z can be an indicator of the dispersion state of filler.

Apart from R_z, R_a is another important parameter to consider. The decrease in R_a with increasing R_z may seem contradicting however can be explained on the basis of observed fractured patterns and surface roughness charts. When treated with 1200P abrasive paper and velvet cloth, no crater was formed due to which lower R_z value was observed. In addition, cracks were deflected quite sharply resulting in sudden variation in surface roughness thereby increasing the R_a value. On the contrary, when treated with 60P and 320P abrasive papers, deep notches were present that caused fracture and increased R_z due to crater formation. However, once crack was formed, it could not deflect much and rest of the fractured surface remained flat thereby decreasing the R_a value. Therefore, a high value of R_a (with low R_z value) can be on indicator of smoother samples surfaces, absence of agglomerates and uniform dispersion of nanofillers. On the other hand, a low value of R_a (with high R_z value) indicates the presence of deep surface notches, agglomerates, and non-uniform dispersion of nanofillers. A similar trend was observed in R_q values as in R_a values. However, no specific trend was observed in surface waviness and may not be indicative of dispersion state of nanofillers and topographical features.

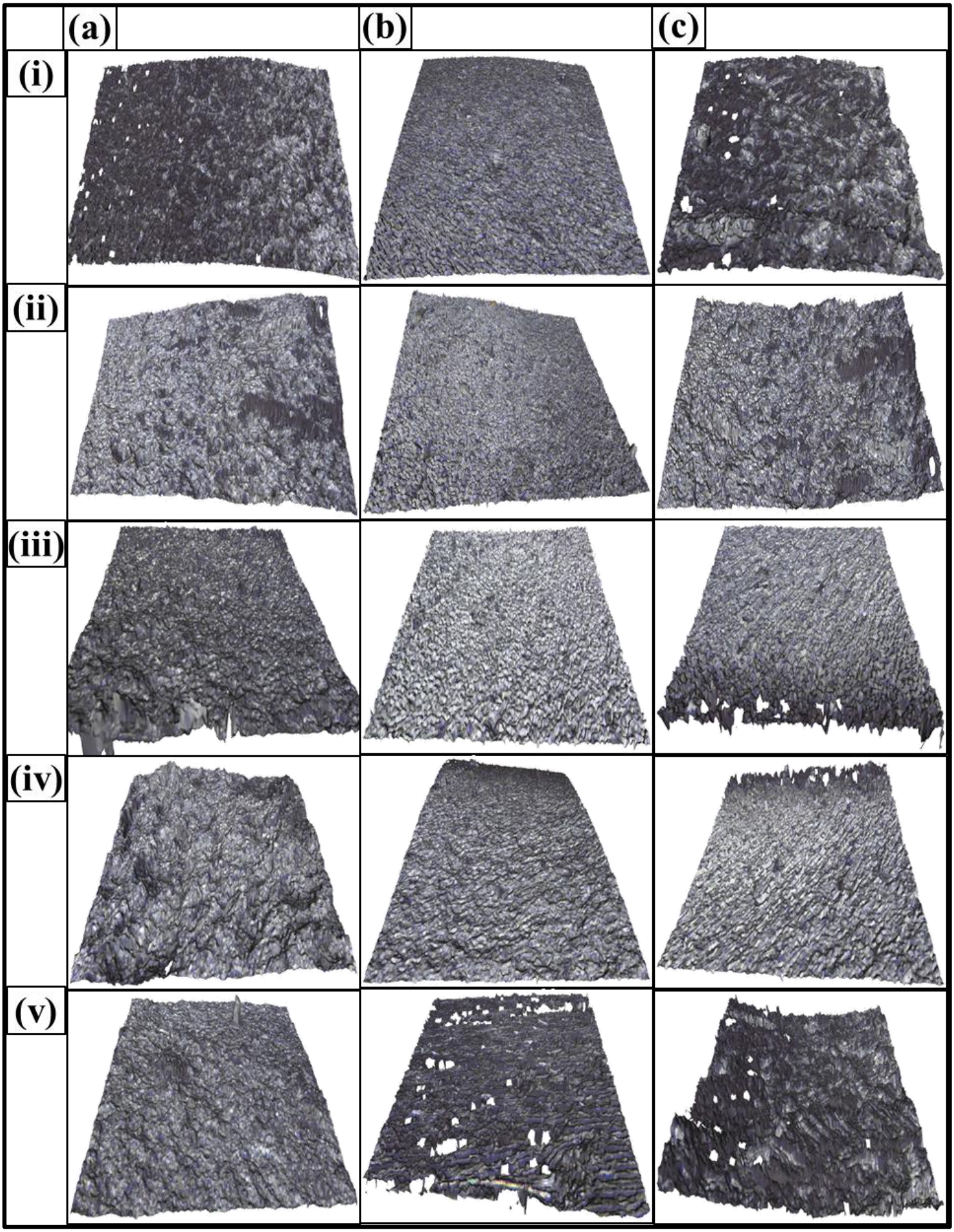

Figure 2: Fractured surfaces of (a) 3PBT, (b) K_{1C}, and (c) Charpy impact test specimens of 1.0 wt% MLG-EP samples. From top to bottom: (i) as-cast, treated with (ii) velvet cloth, (iii) 1200P, (iv) 320P, and (v) 60P. The length of bottom edge of each image is 800 nm.

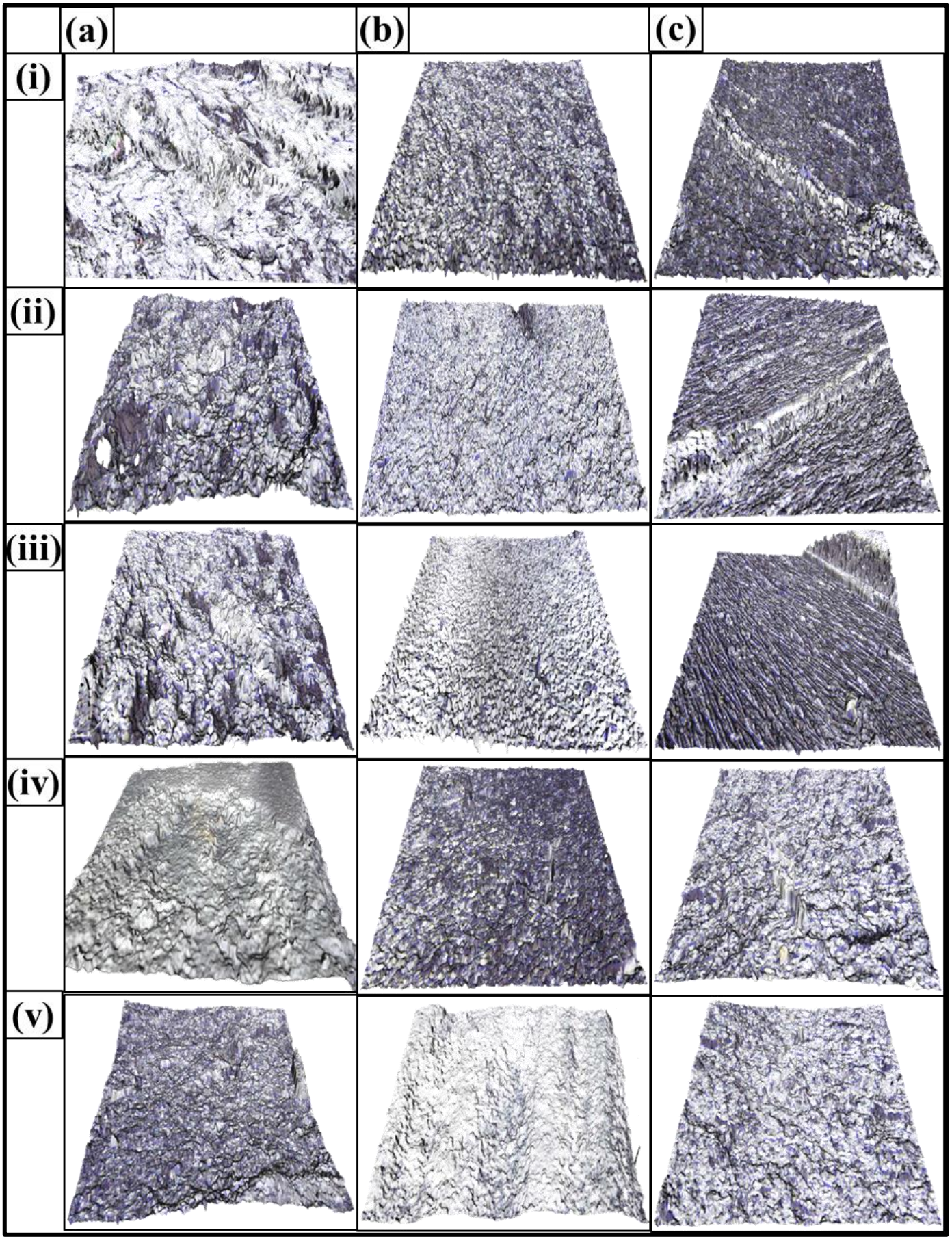

Figure 3: Fractured surfaces of (a) 3PBT, (b) K_{1C}, and (c) Charpy impact test specimens of 1.0 wt% clay-EP samples. From top to bottom: (i) as-cast, treated with (ii) velvet cloth, (iii) 1200P, (iv) 320P, and (v) 60P. The length of bottom edge of each image is 800 nm.

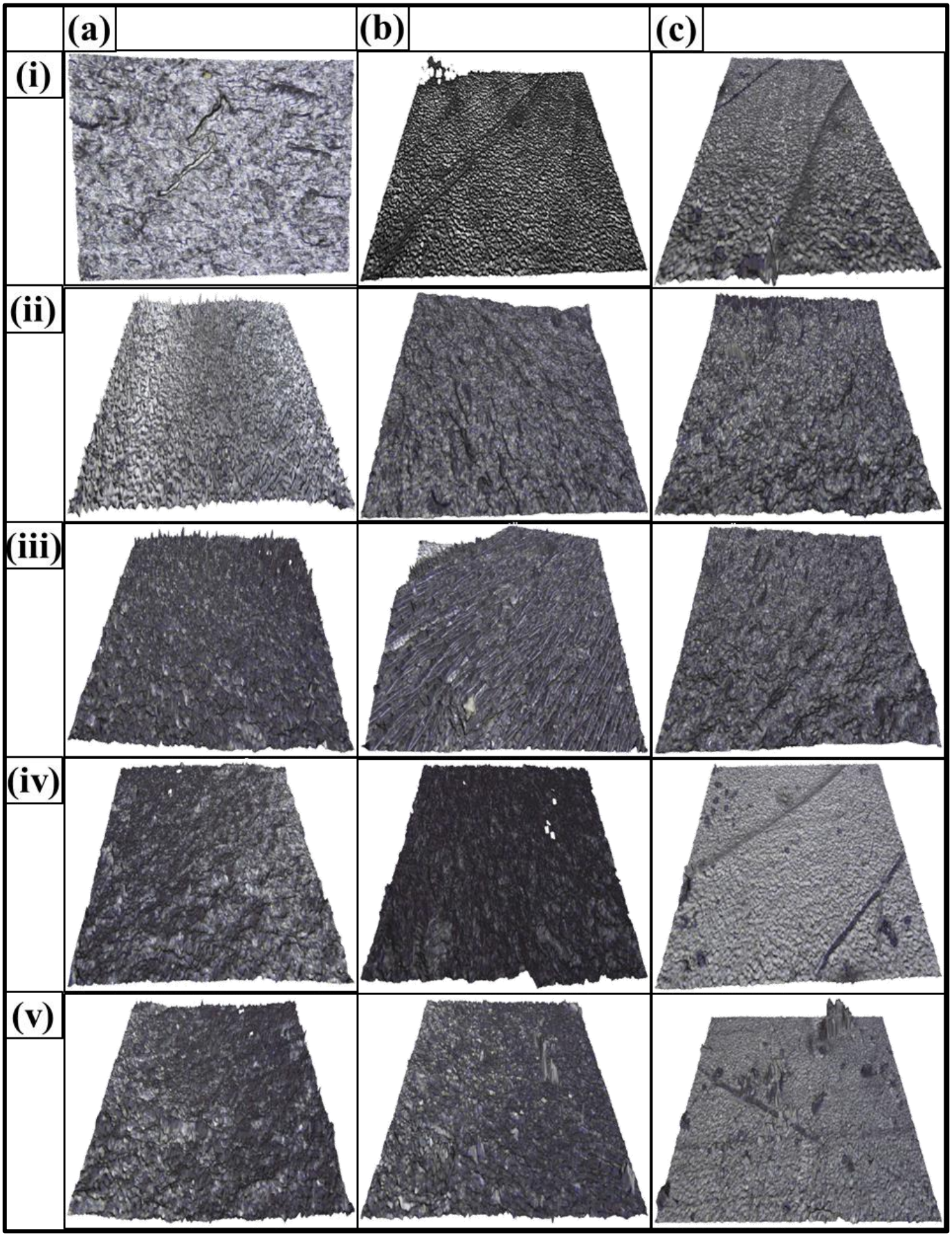

Figure 4: Fractured surfaces of (a) 3PBT, (b) K_{1C}, and (c) Charpy impact test specimens of 0.5 wt% MLG-0.5 wt% clay-EP samples. From top to bottom: (i) as-cast, treated with (ii) velvet cloth, (iii) 1200P, (iv) 320P, and (v) 60P. The length of bottom edge of each image is 800 nm.

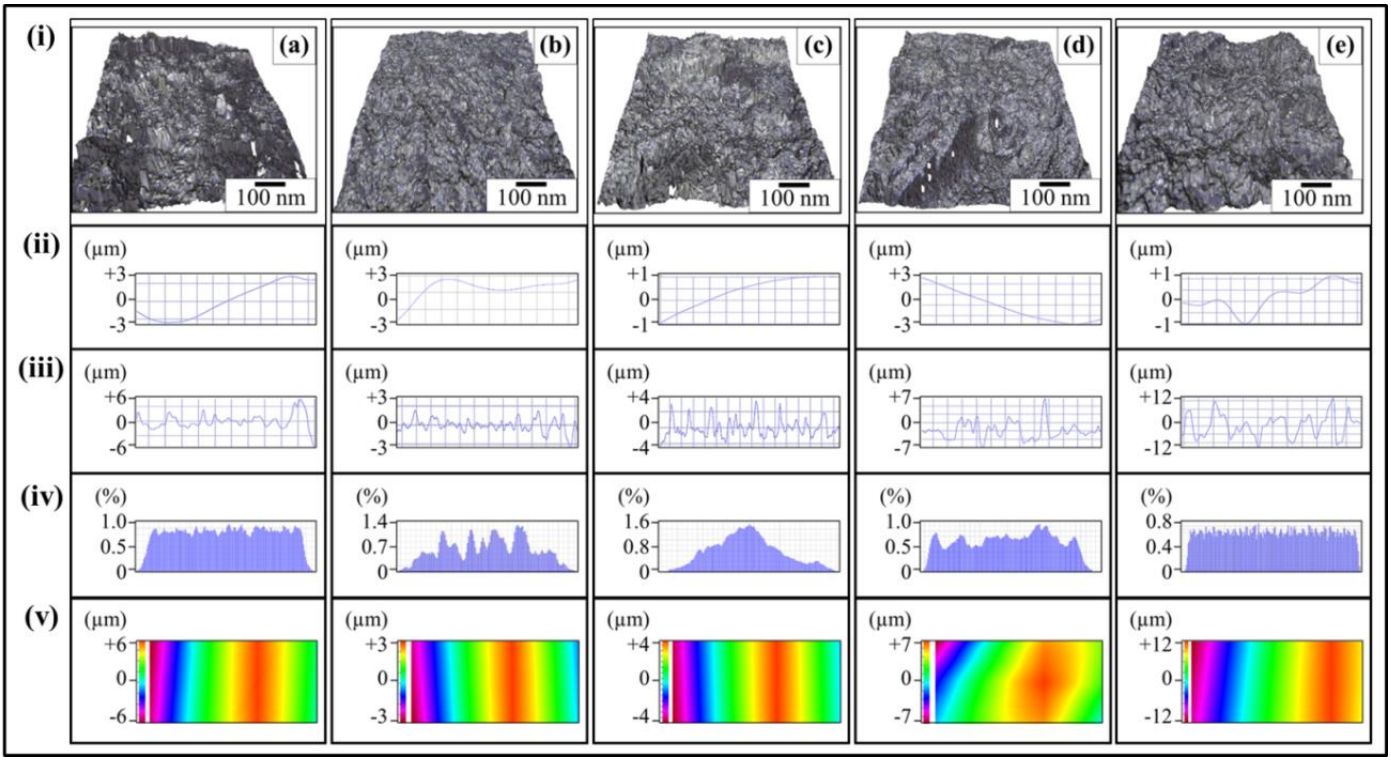

Figure 5: Topographical features of 1.0 wt% MLG-EP fractured tensile samples: (a) as-cast, treated with (b) velvet cloth, (c) 1200P, (d) 320P, and (e) 60P. From top to bottom: (i) tensile images (ii) waviness, (iii) surface roughness, (iv) Gaussian distribution, and (v) surface profile.

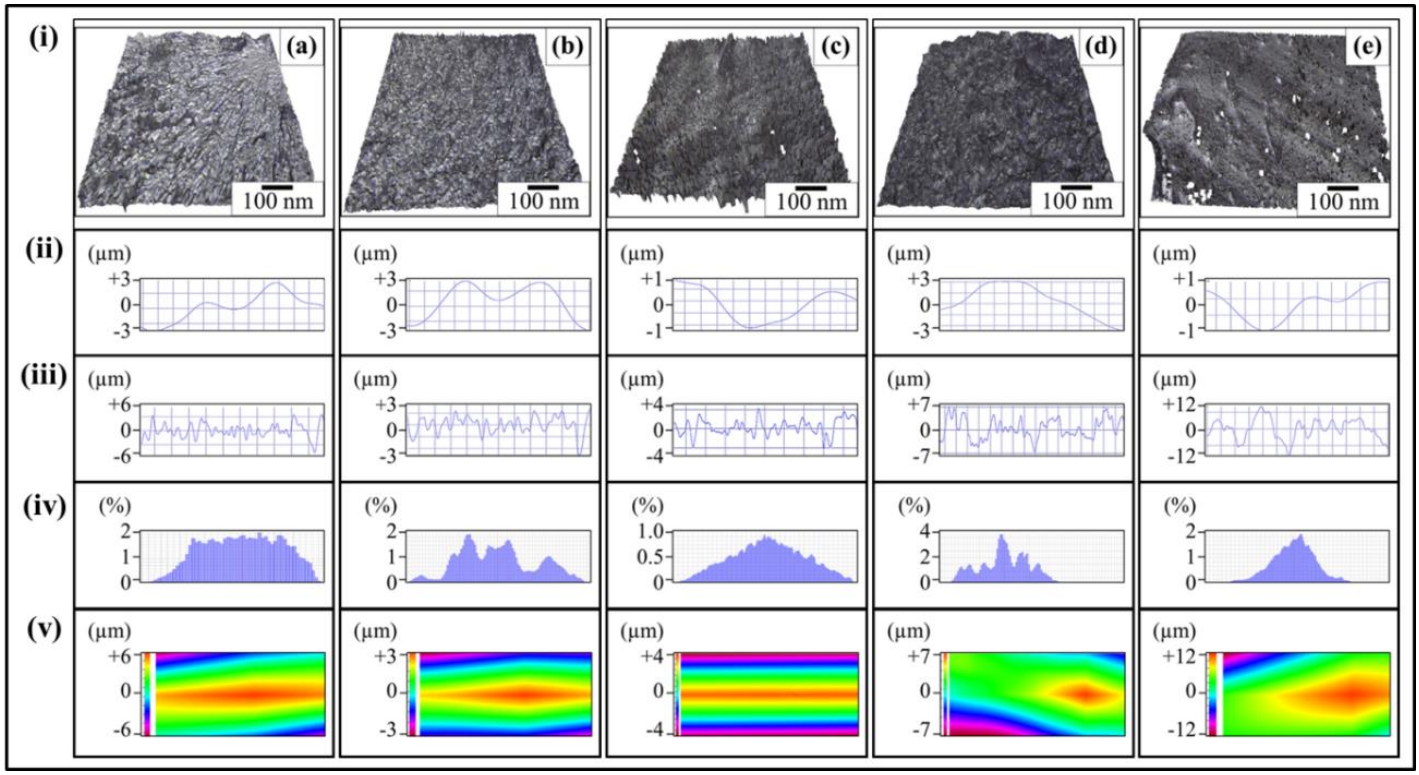

Figure 6: Topographical features of 1.0 wt% clay-EP fractured tensile samples: (a) as-cast, treated with (b) velvet cloth, (c) 1200P, (d) 320P, and (e) 60P. From top to bottom: (i) tensile images (ii) waviness, (iii) surface roughness, (iv) Gaussian distribution, and (v) surface profile.

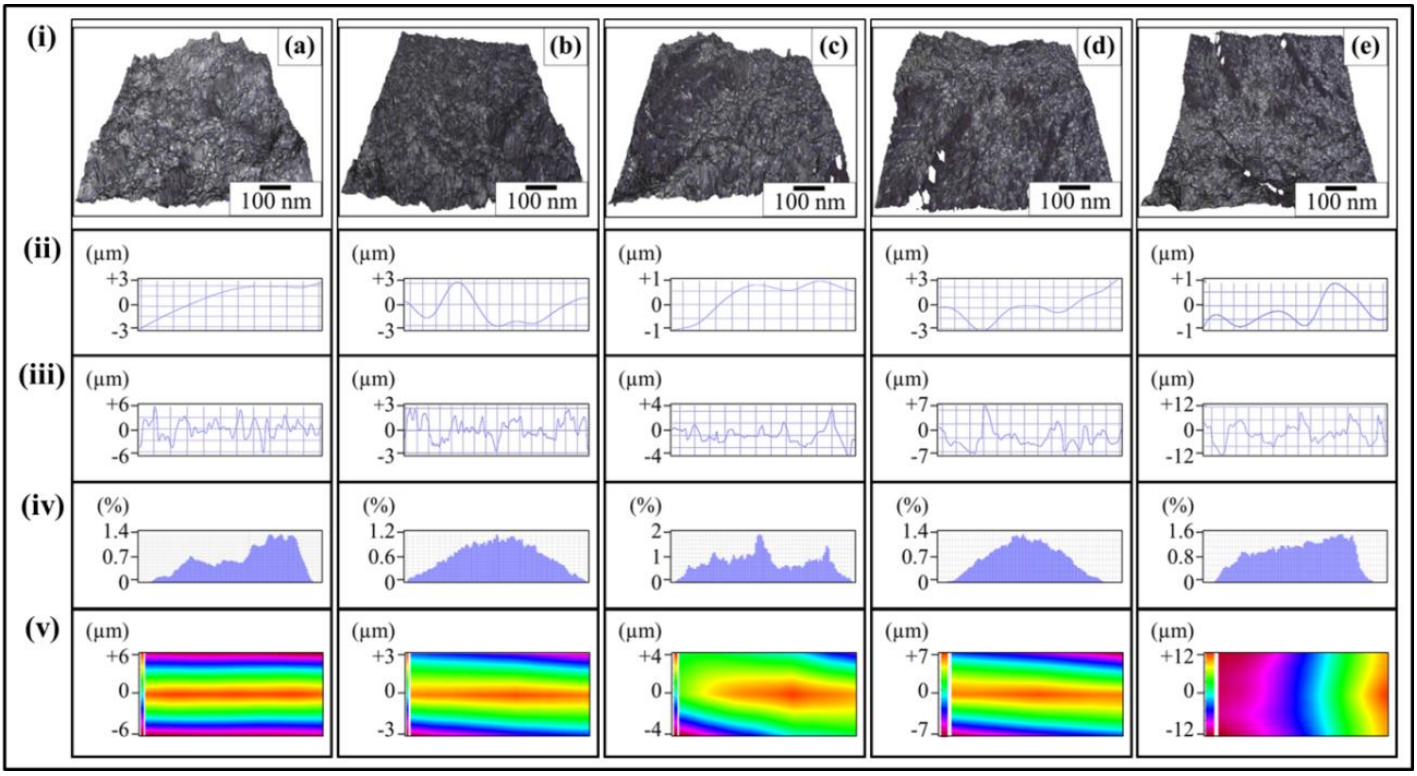

Figure 7: Topographical features of 0.5 wt% MLG-0.5 wt% clay-EP fractured tensile samples: (a) as-cast, treated with: (b) velvet cloth, (c) 1200P, (d) 320P, and (e) 60P. From top to bottom: (i) tensile images (ii) waviness, (iii) surface roughness, (iv) Gaussian distribution, and (v) surface profile.

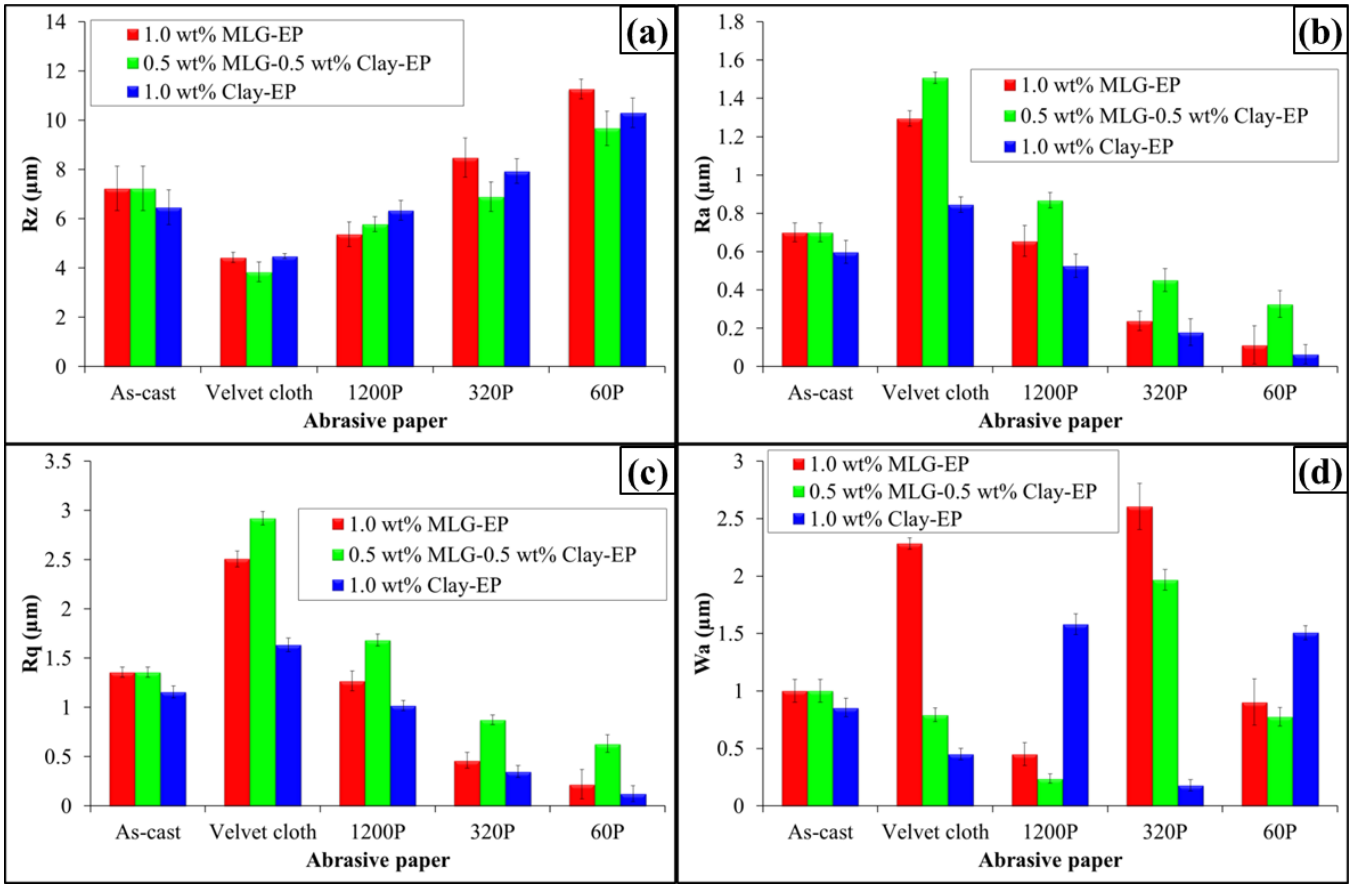

Figure 8: Topographical features of tensile specimens of 1.0 wt% MLG/clay-EP samples.

4 Conclusions:

In conclusion, the topographical features of fractured patterns of polymer nanocomposites can be used to approximate the dispersion state, interfacial interactions, and presence of agglomerates, and overall influence of the incorporation of fillers on the mechanical properties of produced nanocomposites. A high value of R_a (with low R_z value) can be on indicator of smoother samples surfaces, absence of agglomerates and uniform dispersion of nanofillers. On the other hand, a low value of R_a (with high R_z value) indicates the presence of deep surface notches, agglomerates, and non-uniform dispersion of nanofillers. A similar trend was observed in R_q values as in R_a values. However, no specific trend was observed in surface waviness and may not be indicative of dispersion state of nanofillers and topographical features.

5 Acknowledgements:

The authors would like to thank the Department of Mechanical and Construction Engineering, Northumbria University, UK for the provision of research facilities, without which the analysis of relevant data was not possible.

6 References:

[1] Carlson R. L., Kardomateas G. A., Craig J. I. Mechanics of Failure Mechanisms in Structures. 1st ed. springer; 2012.

[2] Atif R, Inam F. Reasons and remedies for the agglomeration of multilayered graphene and carbon nanotubes in polymers. Beilstein J Nanotechnol 2016;7:1174–96. doi:10.3762/bjnano.7.109.

[3] Atif R, Shyha I, Inam F. The degradation of mechanical properties due to stress concentration caused by retained acetone in epoxy nanocomposites. RSC Adv 2016;6:34188–97. doi:10.1039/C6RA00739B.

[4] Miracle DB, Donaldson SL, editors. ASM Handbook Vol. 21, Composites. 2001.

[5] Atif R, Inam F. Modeling and Simulation of Graphene Based Polymer Nanocomposites : Advances in the Last Decade. Graphene 2016:96–142. doi:http://dx.doi.org/10.4236/graphene.2016.52011.

[6] Atif R, Shyha I, Inam F. Modeling and experimentation of multi-layered nanostructured graphene-epoxy nanocomposites for enhanced thermal and mechanical properties. J Compos Mater 2016:1–12. doi:10.1177/0021998316640060.

[7] Atif R, Wei J, Shyha I, Inam F. Use of morphological features of carbonaceous materials for improved mechanical properties of epoxy nanocomposites. RSC Adv 2016;6:1351–9. doi:10.1039/C5RA24039E.

[8] Yao XF, Zhou D, Yeh HY. Macro/microscopic fracture characterizations of SiO2/epoxy nanocomposites. Aerosp Sci Technol 2008;12:223–30. doi:10.1016/j.ast.2007.03.005.

[9] Wetzel B, Rosso P, Haupert F, Friedrich K. Epoxy nanocomposites - fracture and toughening mechanisms. Eng Fract Mech 2006;73:2375–98. doi:10.1016/j.engfracmech.2006.05.018.

[10] Naous W, Yu XY, Zhang QX, Naito K, Kagawa Y. Morphology, tensile properties, and fracture toughness of epoxy/Al2O3 nanocomposites. J Polym Sci Part B-Polymer Phys 2006;44:1466–73. doi:10.1002/Polb.20800.

[11] Kim BC, Park SW, Lee DG. Fracture toughness of the nano-particle reinforced epoxy composite. Compos Struct 2008;86:69–77. doi:10.1177/0892705714556835.

[12] Wang K, Chen L, Wu J, Toh ML, He C, Yee AF. Epoxy nanocomposites with highly exfoliated clay: Mechanical properties and fracture mechanisms. Macromolecules 2005;38:788–800. doi:10.1021/ma048465n.

[13] Liu W, Hoa S V., Pugh M. Fracture toughness and water uptake of high-performance epoxy/nanoclay nanocomposites. Compos Sci Technol 2005;65:2364–73. doi:10.1016/j.compscitech.2005.06.007.

[14] Gojny FH, Wichmann MHG, Köpke U, Fiedler B, Schulte K. Carbon nanotube-reinforced epoxy-composites: Enhanced stiffness and fracture toughness at low nanotube content. Compos Sci Technol 2004;64:2363–71. doi:10.1016/j.compscitech.2004.04.002.

[15] Yu N, Zhang ZH, He SY. Fracture toughness and fatigue life of MWCNT/epoxy composites. Mater Sci Eng A 2008;494:380–4. doi:10.1016/j.msea.2008.04.051.

[16] Srikanth I, Kumar S, Kumar A, Ghosal P, Subrahmanyam C. Effect of amino functionalized MWCNT on the crosslink density, fracture toughness of epoxy and mechanical properties of carbon-epoxy composites. Compos Part A Appl Sci Manuf 2012;43:2083–6. doi:10.1016/j.compositesa.2012.07.005.

[17] Mathews MJ, Swanson SR. Characterization of the interlaminar fracture toughness of a laminated carbon/epoxy composite. Compos Sci Technol 2007;67:1489–98. doi:10.1016/j.compscitech.2006.07.035.

[18] Arai M, Noro Y, Sugimoto K ichi, Endo M. Mode I and mode II interlaminar fracture toughness of CFRP laminates

toughened by carbon nanofiber interlayer. Compos Sci Technol 2008;68:516–25. doi:10.1016/j.compscitech.2007.06.007.
[19] Wong DWY, Lin L, McGrail PT, Peijs T, Hogg PJ. Improved fracture toughness of carbon fibre/epoxy composite laminates using dissolvable thermoplastic fibres. Compos Part A Appl Sci Manuf 2010;41:759–67. doi:10.1016/j.compositesa.2010.02.008.
[20] Cotell CM, Sprague JA, Smidth FAJ, editors. ASM Handbook, Vol. 5. Surface Engineering. 1994.
[21] Kuo W-S, Tai N-H, Chang T-W. Deformation and fracture in graphene nanosheets. Compos Part A Appl Sci Manuf 2013;51:56–61. doi:10.1016/j.compositesa.2013.03.020.